Clim Dyn (2011) 37:2481–2493
DOI 10.1007/s00382-011-1000-x

Future changes in the East Asian rain band projected by global atmospheric models with 20-km and 60-km grid size

Shoji Kusunoki · Ryo Mizuta · Mio Matsueda

Received: 4 June 2010 / Accepted: 17 January 2011 / Published online: 6 March 2011

Abstract Global warming projection experiments were conducted using a 20-km mesh global atmospheric model, focusing on the change in the rain band of East Asian summer monsoon. To assess the uncertainty of climate change projections, we performed ensemble simulations with the 60-km resolution model combining four different SSTs and three atmospheric initial conditions. In the present-day climate simulations, the 20-km model reproduces the rain band of East Asian summer monsoon better than lower resolution models in terms of geographical distribution and seasonal march. In the future climate simulation by the 20-km model, precipitation increases over the Yangtze River valley in May through July, Korean peninsula in May, and Japan in July. The termination of rainy season over Japan tends to be delayed until August. Ensemble simulations by the 60-km model show that precipitation in the future climate for July increases over the Yangtze River valley, the East China Sea and Japan. These changes in precipitation are partly consistent with those projected by the 20-km model. Simulations by the 20-km and 60-km models consistently show that in the future climate the termination of rainy season over Japan tends to be delayed until August. The changes in the vertically integrated water vapor flux show the intensification of clockwise moisture transport over the western Pacific subtropical high. Most precipitation changes over the East Asia can be interpreted as the moisture convergence resulting from change in the horizontal transport of water vapor.

Keywords Climate change · East Asian summer monsoon · High horizontal resolution global atmospheric model

S. Kusunoki (✉) · R. Mizuta
Climate Research Department, Meteorological Research Institute, 1-1, Nagamine, Tsukuba, Ibaraki 305-0052, Japan
e-mail: skusunoki@mri-jma.go.jp

M. Matsueda
Japan Agency for Marine-Earth Science and Technology (JAMSTEC), Tsukuba, Ibaraki 305-0052, Japan

1 Introduction

The rainy season or rain band observed in an East Asian summer monsoon season is called the Baiu in Japan, the Mei-yu in China and the Changma in Korea. This rainy season begins nearly simultaneously with the onset of the summer monsoon over central India in early June. During this rainy season, the rain band or rain front stagnates over the Yangtze River valley, with its eastern edge passing through the Japan Islands (Ninomiya and Akiyama 1992). The rain band migrates northward with seasonal march and the rainy season terminates in mid-July (Wang and Ho 2002). Hereafter, we will use the terminology "the Baiu rain band" to denote this rain band or associated frontal structure extending over the East Asia in the summer monsoon season. We also will use the terminology "the Baiu season" to denote the period in which the Baiu rain band prevails. The rainy season in East Asia is characterized by this frontal structure of rain band, whereas Indian summer monsoon does not have such frontal structure.

Kusunoki et al. (2006) indicated the realistic reproduction of Baiu rain band needs an atmospheric model with higher horizontal resolution. They investigated the future change in the Baiu rain band with a 20-km mesh global atmospheric model (the 20-km model), using the time-slice method (Bengtsson et al. 1996) which prescribes sea

surface temperature (SST) simulated by an atmosphere–ocean general circulation model (AOGCM).

It is widely recognized that global warming projections include wide range of uncertainty arising from many factors such as differences in future emission scenario, model performance, internal natural variability of climate system. Therefore, evaluation and quantification of uncertainty in global warming projection is strongly required to obtain more robust and reliable information on future climate changes (IPCC 2007). Although the time-slice experiments of the 20-km model are largely affected by prescribed SST, Kusunoki et al. (2006) have used only one set of SSTs for the present-day and future climate simulations. In order to evaluate and quantify uncertainty of the projected change in the Baiu rain band originating from the differences in SSTs prescribed to the 20-km model, Kusunoki and Mizuta (2008) have shown that precipitation increase over the Yangtze River valley and delay in the termination of the Baiu season over Japan were consistently found in the simulations regardless of different SSTs. However, their experiments had limitations. The integration time was 20 years for the longest simulation. Only two AOGCM were selected for prescribing future SSTs.

The purpose of the present study is to investigate the future change in the East Asian summer monsoon by the 20-km model, quantifying the uncertainty of the projection by ensemble simulations with a 60-km mesh model (the 60-km model) for different SST distributions and different atmospheric initial conditions. Kitoh et al. (2009) reported the preliminary results by global warming projection with the 20-km and 60-km models focusing on the change in tropical cyclone, but they have not investigated the changes in the East Asian summer monsoon. In this paper we will describe the changes in the East Asian summer monsoon in detail.

Section 2 describes specifications of the model. Section 3 explains the experimental design. Section 4 describes validation data for precipitation. Section 5 verifies the precipitation climatology in the present-day climate simulations. Section 6 shows the future change projected by the 20-km model. Section 7 represents the future change projected by ensemble simulations with the 60-km model. Section 8 discusses the reason for the future change in precipitation distribution. The paper is concluded in Sect. 9.

2 Models

The AGCM used in this study is called MRI-AGCM3.1S which is jointly developed by the Japan Meteorological Agency (JMA) and the Meteorological Research Institute (MRI). The model is based on an operational numerical weather prediction model used at JMA. Some modifications were added in radiation and land surface processes as a climate model at MRI (Mizuta et al. 2006). The time integration was accelerated by introducing a semi-Lagrangian three-dimensional advection scheme (Yoshimura and Matsumura 2005). The model has a horizontal spectral truncation of TL959 corresponding to about a 20-km horizontal grid spacing and has 60 levels with a 0.1 hPa (altitude of about 65 km) top. TL959 means that the model has a spectral triangular truncation of spherical function at wave number 959 with a linear grid for wave-to-grid transformation. The model has 1920 grids in longitude and 960 grids in latitude. A mere increase in the horizontal resolution was found to gives rise to large model biases in precipitation and temperature, much less organization of convection, and suppression of tropical cyclone generation. Therefore, we carefully tuned the model to improve the model's present-day climatology by changing the parameters in the evaporation process, cloud water content diagnosis, vertical transport of horizontal momentum in cumulus, and gravity wave drag (Mizuta et al. 2006). Especially, over estimation of global average precipitation of the 20-km model was suppressed by decreasing the amount of detrainment of cloud water at the top of the cumulus, as well as decreasing transformation speed from cloud water to precipitation in the cloud scheme (Mizuta et al. 2006). The version of the 20-km model used in this study is slightly different from MRI-AGCM3.0S used in the previous studies (Kusunoki et al. 2006; Kusunoki and Mizuta 2008) in that sea ice model and vegetation setting in land surface process are improved.

To examine the dependence of horizontal resolution on the reproducibility of the present-day climatology, we also performed simulations with three lower spatial resolutions, using the same model framework (Mizuta et al. 2006). The resolutions are TL319L60 (640 grids in longitude, 320 grids in latitude, about 60 km in grid size, and 60 vertical levels up to 0.1 hPa), TL159L40 (320, 160 grids, 120 km, 40 levels, 0.4 hPa top), and TL95L40 (192, 96 grids, 180 km, 40 levels, 0.4 hPa top). In these additional simulations, the parameter adjustments introduced to the 20-km model (TL959L60, 1920, 960 grids, 60 levels, 0.1 hPa top) were not included, but the modification on the vertical transport of the horizontal momentum was included.

The 60-km model (MRI-AGCM3.1H) was used for ensemble simulations to estimate and quantify uncertainty of future projections. The integration of the models and data processing were performed on the Earth Simulator (Habata et al. 2004).

3 Experimental design

3.1 Present-day climate simulations

The time-slice experiment (Bengtsson et al. 1996) was conducted as follows. Figure 1 shows a schematic diagram

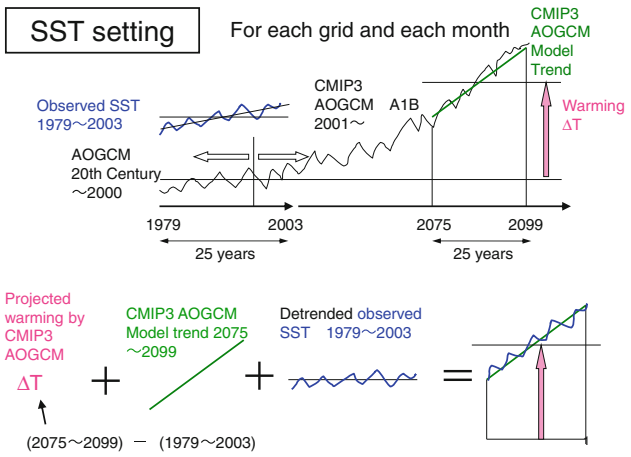

Fig. 1 A schematic diagram of sea surface temperatures (SST)s given to the 20-km model. These calculations were applied to each grid and each month

of SST setting. Table 1 summarizes the specification of simulations. For the present-day climate simulation, the 20-km model was integrated for 25 years from 1979 to 2003 (run name SP) with the observed historical sea surface temperature (SST) and sea ice data of HadISST1 (Rayner et al. 2003). This simulation is equivalent to an Atmospheric Model Intercomparison Project (AMIP)-type experiment for an atmospheric model, which is widely adopted in numerous modeling studies. Similar simulations were conducted with the 60-km model (HP), the 120-km model (MP) and the 180-km model (LP). As for the 60-km model, three-member ensemble simulations with different atmospheric initial conditions were performed to evaluate the internal variability of model atmosphere.

3.2 Future climate simulations by the 20-km model

For the future climate simulations, the 20-km model was integrated for 25 years from 2075 to 2099 with future SSTs (SF). The boundary SST data were prepared by superposing; (a) future change in the multi-model ensemble (MME) of SST projected by Coupled Model Intercomparison Project phase 3 (CMIP3) multi-model dataset, (b) the linear trend in MME of SST projected by CMIP3 multi-model dataset and (c) the detrended observed SST anomalies for the period 1979–2003. Future change in MME of SST was evaluated by the difference between the 20th Century experiment (20C3M) of Intergovernmental Panel on Climate Change (IPCC) Fourth Assessment Report (AR4; IPCC 2007) and future simulation under the Special Report on Emission Scenario (SRES) A1B emission scenario (IPCC 2000). Future sea-ice distribution is obtained in a similar fashion. Details of the method are described in Mizuta et al. (2008). The design retains observed year-to-year variability and El Niño and Southern Oscillation (ENSO) events in the future climate, but with a higher mean and clear increasing trend in SST. This is a reasonable assumption, because IPCC AR4 (2007) drew no definitive conclusion on the change in ENSO judging from large uncertainties in the future projections by

Table 1 Experimental design

Target period	Year (25 years)	Grid size (km)	Run name[a]	Sea surface temperature	Ensemble size of atmospheric initial condition
Present-day	1979–2003	20	SP	Observation HadISST1[b]	1
	1979–2003	60	HP	Observation HadISST1	3
	1979–2003	120	MP	Observation HadISST1	1
	1979–2003	180	LP	Observation HadISST1	1
Future	2075–2099	20	SF	CMIP3[c] multi-model ensemble	1
	2075–2099	60	HF	CMIP3 multi-model ensemble	3
	2075–2099	60	HF CSIRO	CSIRO-MK3.0[d]	3
	2075–2099	60	HF MIROC	MIROC3.2(hires)[e]	3
	2075–2099	60	HF MRI	MRI-CGCM2.3.2[f]	3

[a] Thirst character of run name denotes horizontal resolution: *S* Super high (20 km), *H* High (60 km), *M* Medium (120 km), *L* Low (180 km). Second character of run name denotes target period: *P* Present-day, *F* Future

[b] Observational data by the Hadley Center of Met Office, United Kingdom (Rayner et al. 2003)

[c] Coupled Model Intercomparison Project 3

[d] Commonwealth Scientific and Industrial Research Organization (CSIRO) Atmospheric Research

[e] Center for Climate System Research (University of Tokyo), National Institute for Environmental Studies, and Frontier Research Center for Global Change (FRCGC) of Japan Agency for Marine-Earth Science and Technology (JAMSTEC), Japan

[f] Meteorological Research Institute, Japan

AOGCMs. The changes in global annual mean SST at the end of the 21st century (2075–2099) from the present-day climate (1979–2003) is 2.17°C.

3.3 Ensemble simulations by the 60-km model for the future climate

Considering that the time-slice experiments of the 20-km model are largely affected by prescribed SST, it is desirable that uncertainty of future projections should be evaluated by the ensemble simulations of the 20-km model forced with different SSTs. However, owing to the limitation of computer resource, we have to use the 60-km model for ensemble simulations. Computational time of the 20-km model is twenty times larger than that of the 60-km model. As a measure of future change in SST projected by AOGCMS, we have selected two metrics. One is the effective climate sensitivity ΔT which is defined by the change in global average annual surface air temperature at the time of doubled CO_2 concentration, considering the delay of ocean warming (IPCC 2007, Table S8.1). The other is ENSO polarity (El Niño/La Niña) defined by Yamaguchi and Noda (2006). We have tried to widely sample the AOGCM model in the two-dimensional phase space spanned by the effective climate sensitivity and the ENSO polarity. We have adopted the SST distributions of three specific AOGCMs; CSIRO_MK3.0 ($\Delta T = 2.21$°C, El Niño like), MIROC3.2(hires) ($\Delta T = 5.87$°C, La Niña like) and MRI-CGCM2.3.2 ($\Delta T = 2.97$°C, El Niño like). The average of ΔT for nineteen CMIP3 AOGCMs is 2.93°C. Warming projected by MIROC3.2(hires), MRI-CGCM2.3.2 and CSIRO_MK3.0 is large, intermediate, small among CMIP3 AOGCMs, respectively. Figure 2 shows the example of four different SST distributions. SSTs are the functions of grid, month and year. We also confirmed that these three AOGCMs show relatively higher reproducibility of summer (June to August) precipitation climatology over the East Asia region among CMIP3 AOGCMs (Kitoh and Uchiyama 2006). In order to evaluate the internal variability of model atmosphere, we have also conducted three-member ensemble simulations with different atmospheric initial conditions for each SST distributions.

4 Validation data of precipitation

To verify the precipitation climatology in the present-day climate simulation (1979 to 2003, 25 years), five different observational data are used. We need high horizontal resolution observation to validate the 20-km model, but such data have some restrictions in data coverage of time and space. We used conventional dataset for model validation as well as observations with high horizontal resolution.

4.1 GPCP 2.5 degree

The first one is the Global Precipitation Climatology Project (GPCP) compiled by Adler et al. (2003). The horizontal resolution is 2.5° in longitude and latitude, corresponding to a grid spacing of about 210 km over Japan. Monthly and pentad data cover the whole period of the present-day climate simulation (1979–2003). This dataset is widely used to verify the climate models, but the horizontal resolution is much lower than that of the 20-km model.

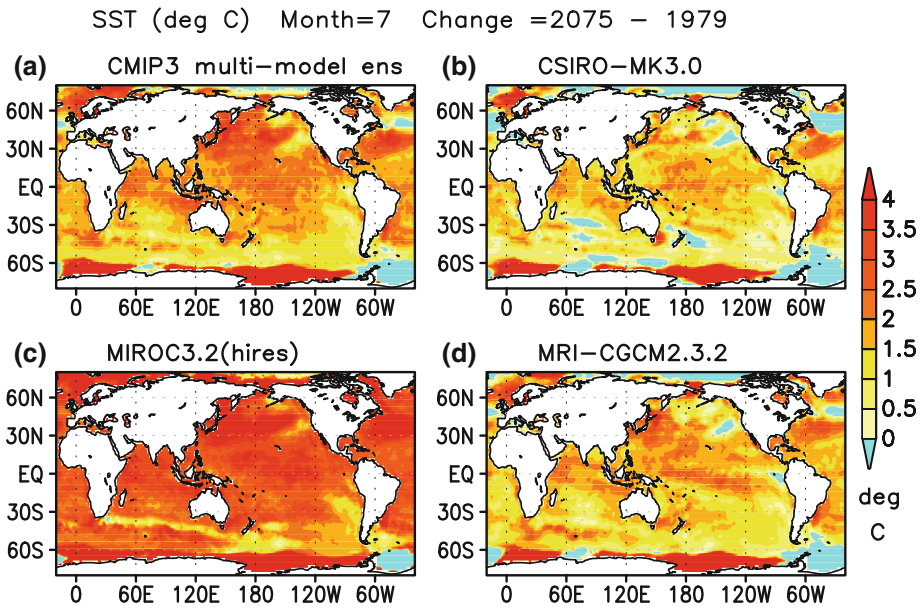

Fig. 2 SST changes prescribed to the 60-km model for July 2075. SST differences between July 2075 and July 1979 were shown. SST depends on grid, month and year. **a** SST projected by the CMIP3 multi-model ensemble. **b** CSIRO-MK3.0. **c** MIROC3.2(hires). **d** MRI-CGCM2.3.2

4.2 GPCP 1DD

The second one is the One-Degree Daily (1DD) data of GPCP V1.1 compiled by Huffman et al. (2001). Horizontal resolution is one degree in longitude and latitude, corresponding to a grid spacing of about 90 km over Japan. These data are more appropriate for evaluating the small-scale structure of the 20-km model than conventional 2.5-degree resolution data, although the data cover only 12 years from 1997 to 2008.

4.3 TRMM

The third one is the Tropical Rainfall Measuring Mission (TRMM) data compiled by Huffman et al. (2007). Horizontal resolution is 0.25° in longitude and latitude, corresponding to a grid spacing of about 25 km over Japan. The data cover only 11 years from 1998 to 2008 in a global belt extending from 50°S to 50°N. The 3B42 products are based on 3-hourly infrared precipitation estimates calibrated and combined with microwave precipitation estimates. We used the 3B42 products to verify the time evolution of precipitation in a pentad resolution. The 3B43 products are monthly data derived from 3-hourly infrared precipitation estimates calibrated and combined with rain gauge estimates. We used the 3B43 products to verify the monthly data of precipitation.

4.4 APHRODITE

The fourth one is the Asian Precipitation Highly Resolved Observational Data Integration Towards the Evaluation of Water Resources (APHRODITE) Version 0902 data compiled by Yatagai et al. (2009). APHRODITE is daily gridded precipitation dataset based on rain gauge observations over Asia region. Horizontal resolution is 0.25° in longitude and latitude, corresponding to a grid spacing of about 25 km over Japan. The data cover the whole period of the present-day climate simulation (1979–2003), but region of data is restricted to land.

4.5 CMAP

The fifth one is Climate prediction center Merged Analysis of Precipitation (CMAP) compiled by Xie and Arkin (1997). A dataset without model generated precipitation in the process of data assimilation is used. All data are interpolated to grid points with 2.5-degree resolution in longitude and latitude. The horizontal resolution is 2.5° in longitude and latitude, corresponding to a grid spacing of about 210 km over Japan. The data cover the whole period of the present-day climate simulation. This dataset is also widely used to verify the climate models as well as GPCP 2.5° data.

5 Present-day climate simulations

The first step of the global warming projection is to examine the model's ability to reproduce the present-day climatology. Figure 3 compares the observed and simulated climatological precipitation of July. Four observations with different horizontal resolution and different data coverage in space and time are shown. The 20-km model reproduces the concentration of precipitation over western Japan and the Korean peninsula, but coarser models underestimate precipitation over these regions.

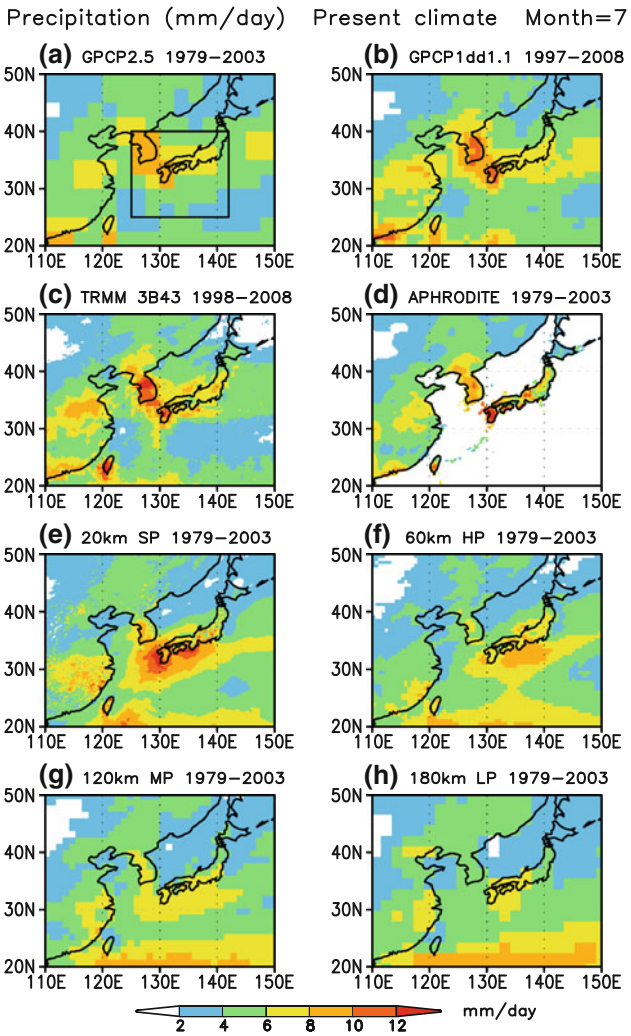

Fig. 3 Observed (**a**–**d**) and simulated (**e**–**h**) climatological precipitation of July. Unit is mm day^{-1}. **a** GPCP (2.5°, 1979–2003, 25 years, Adler et al. 2003).The *box* shows the target region for Fig. 4. **b** GPCP 1DD (1°, 1997–2008, 12 years, Huffman et al. 2001). **c** TRMM 3B43 (0.25°, 1998–2008, 11 years, Huffman et al. 2007). **d** APHRODITE (0.25°, 1979–2003, 25 years, Land only, Yatagai et al. 2009). **e** The 20-km model averaged for 25 years from 1979 to 2003 (SP). **f** The 60-km model (HP). The first run out of simulations with three different atmospheric initial conditions is shown. **g** The 120-km model (MP). **h** The 180-km model (LP)

In Fig. 3 the 60 km model simulation is taken from the first ensemble member out of three ensemble simulations with different atmospheric initial conditions. Differences of geographic distribution among three members of the 60 km model simulations (figure not shown), which can be regarded as internal variability of model atmosphere, are much smaller than differences among the 20, 60, 120 and 180 km model simulations. Spatial correlation coefficient between the first and second member of the 60-km model simulations, that between first and third member, and that between second and third member are 0.949, 0.953 and 0.961, respectively.

In Fig. 4, the observed seasonal marching of precipitation is compared with the model simulations for the longitudinal sector including Japan. The target region is indicated by the box in Fig. 3a. Hokkaido island in Northern Japan (140–145°E, 41–45°N) was excluded because there is no Baiu season there. In the beginning of June, an area of large precipitation is observed around 25–30°N (Fig. 4a–c). This area of heavy rainfall then gradually migrates northward until mid-July and then disappears. This band of northward-migrating rain corresponds to the Japanese rainy season, the Baiu. Lower resolution models (Fig. 4e–g) generally underestimate the amount of precipitation in the Baiu rain band and do not show the northward migration. In contrast, the 20-km model (d) simulates larger precipitation than lower resolution models. Also, the 20-km model shows the northward migration of rain band, although the speed of migration is underestimated. In summary, the 20-km model reproduces the Baiu rain band better than lower resolution models. This is consistent with the previous results of Kusunoki et al. (2006).

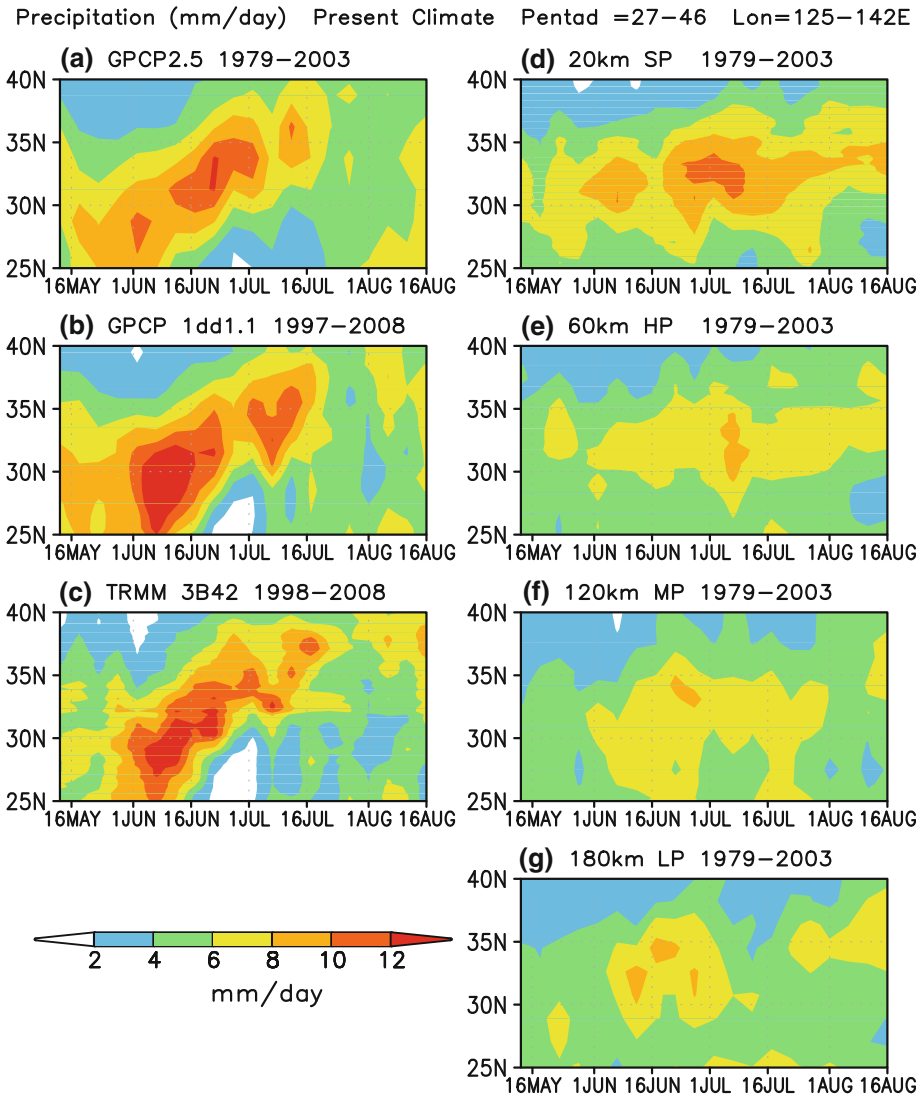

Fig. 4 Time-latitude cross section of the observed (**a**–**c**) and simulated (**d**–**g**) climatological pentad mean precipitation averaged for 125–142°E. The target region is indicated in Fig. 3a. The target period is from pentad 27 (11–15 May) to 46 (14–18 August). Unit is mm day^{-1}. **a** GPCP (2.5°, 1979–2003, 25 years, Adler et al. 2003). **b** GPCP 1DD V1.1(1°, 1997–2008, 12 years, Huffman et al. 2001). **c** TRMM 3B42 (0.25°, 1998–2008, 11 years, Huffman et al. 2007). **d** The 20-km model averaged for 25 years from 1979 to 2003 (SP). **e** The 60-km model (HP). The first run out of simulations with three different atmospheric initial conditions is shown. **f** The 120-km model (MP). **g** The 180-km model (LP)

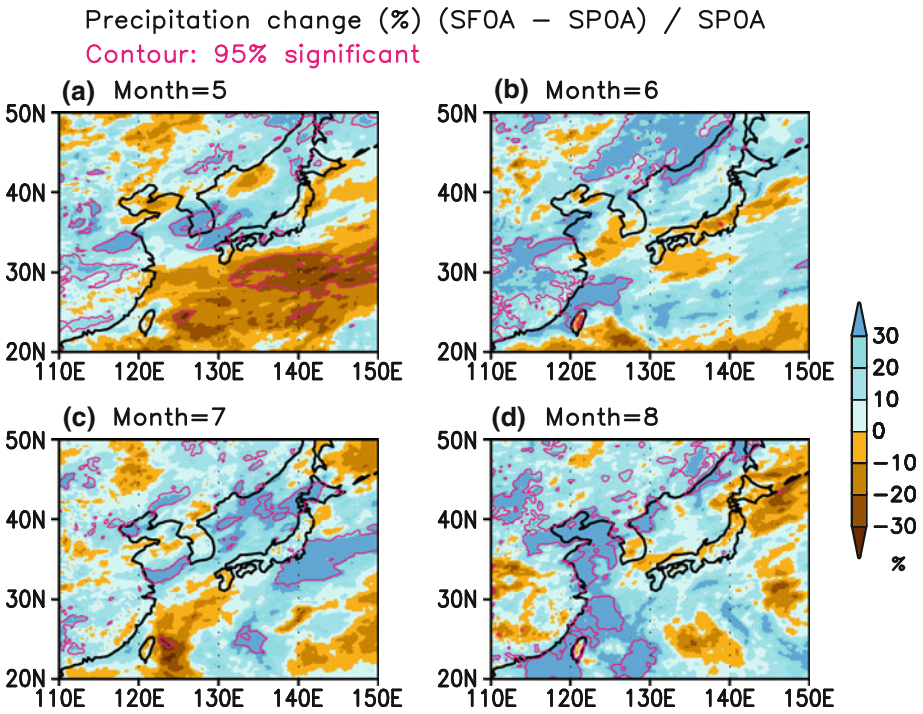

Fig. 5 Future changes in precipitation relative to the present-day climatology by the 20-km model. (SF − SP)/SP. Unit is %. Red contours show the 95% confidence level by a two-sided Student's *t* test. **a** May. **b** June. **c** July. **d** August

In Fig. 4 the 60 km model simulation is taken from the first ensemble member out of three ensemble simulations with different atmospheric initial conditions. Differences of time-latitude cross section among three members of the 60 km model simulations (figure not shown), which can be regarded as internal variability of model atmosphere, are much smaller than differences between the 20-km and 60-km model simulations. In contrast, differences among three members of the 60 km model simulations are almost comparable to differences among the 60-km, 120-km, and 180-km model simulations. Correlation coefficient between the first and second member of the 60-km model simulations, that between first and third member, and that between second and third member are 0.685, 0.744 and 0.684, respectively. These correlation coefficients are lower than those for the case of Fig. 3f (0.949, 0.953 and 0.961), because variability of pentad mean is much larger than that of monthly mean data.

6 Future climate simulations by the 20-km model

Figure 5 illustrates the changes in precipitation over the East Asia region projected by the 20 km model. In May, precipitation increases over the Yangtze River valley of China and the Korean peninsula. On the contrary, precipitation decreases over the ocean to the south of Japan archipelago. In June, precipitation increases over the middle reach of Yangtze River valley in China, but statistically significant changes are not found near Japan. In July, precipitation increases over the East China Sea and around Japan. In August, precipitation increases over the northern part of China, the East China Sea and near Taiwan. From June to August, the area of statistically significant increase is much larger than that of decrease over the whole domain. Focusing on region around Japan, increase in precipitation is largest in July. Kusunoki and Mizuta (2008) investigated the dependence of SST distribution on the future precipitation change by the 20-km model. They indicated the robust precipitation increase over the Yangtze River valley in June (their Fig. S2) and July (their Fig. 2). Our present results also show precipitation increase over the Yangtze River valley in June and July, but change in July is not statistically significant. Since the model and SST setting of the present study are different from those of Kusunoki and Mizuta (2008), simple comparison is not straightforward. Over Japan and Korea, common change was not found in Kusunoki and Mizuta (2008) and in our present study.

Figure 6 depicts changes in the seasonal march of the rain band projected by the 20-km model for three regions. In Japan (Fig. 6a), precipitation decreases in May around 20–30°N which is also confirmed by Fig. 5a. Precipitation increases in July and in the first half of August. Changes are not statistically significant mainly due to large year-to-year variability, but these changes suggest the

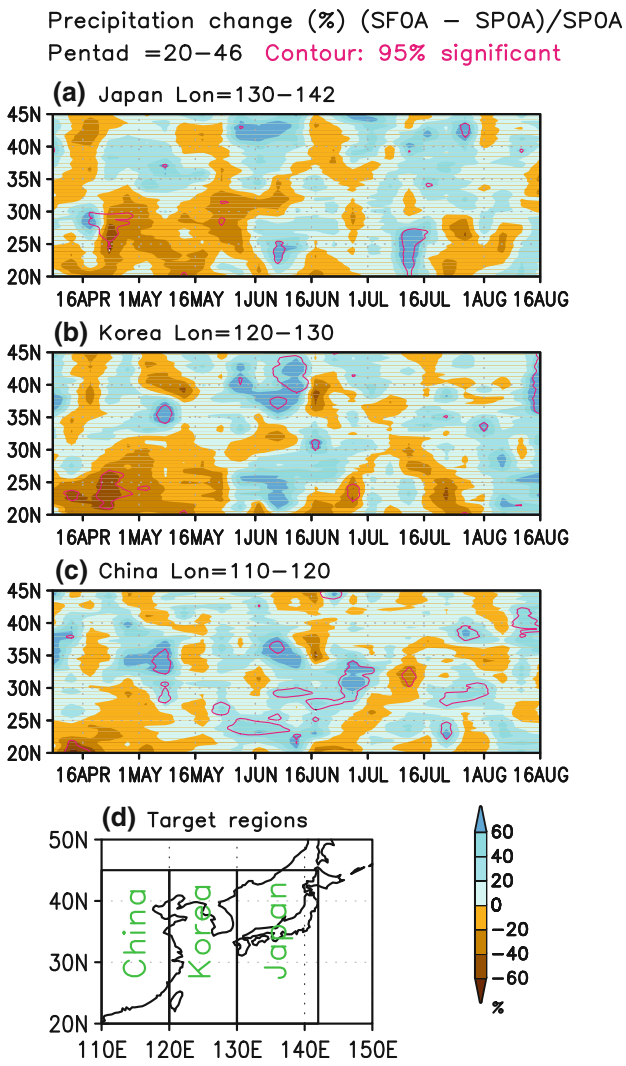

Fig. 6 Time-latitude cross section of future changes in precipitation relative to the present-day climatology by the 20-km model for three target regions. (SF − SP)/SP. Unit is %. The target period is from pentad 20 (6–10 April) to 46 (14–18 August). Red contours show the 95% confidence level. **a** Japan. **b** Korea. **c** China. **d** Definition of target regions

possibility of delay in seasonal march of rainy season. This tendency of delay is consistent with the results of previous studies by CMIP3 AOGCMs (Kitoh and Uchiyama 2006) and by the 20-km model (Kusunoki et al. 2006; Kusunoki and Mizuta 2008). Over Korea corresponding around 35–40°N in Fig. 6b, precipitation increases in the first halves of June and August. Most changes are not statistically significant like Japan case. Over the Yangtze River valley in China corresponding around 30°N in Fig. 6c, statistically significant increase in precipitation are frequently found from May to August. Large increase of precipitation over the Yangtze River valley in June is also confirmed by Fig. 4b.

7 Future climate simulations by the 60-km model

In order to evaluate uncertainty of future projections, ensemble simulations by the 60-km were conducted combining four SST distributions and three atmospheric initial conditions. Figure 7 shows precipitation change in the all twelve simulations for July. The reason why we selected July is that changes in July over Japan are larger than those in other months. The evident feature is that the changes in precipitation are largely affected by the SST distributions rather than initial condition of atmosphere. In other words, differences among simulations with three atmospheric initial conditions are small for the same SST. In the simulations with CMIP3 multi-model ensemble SST (Fig. 7a–c), precipitation increases over the Yangtze River valley, the East China Sea and Japan. In the simulations with CSIRO SST (Fig. 7d–f), precipitation increases over southern part of China, the East China Sea and Japan, which is almost similar to CMIP3 SST case. Decrease of precipitation over the ocean to the south of Japan is larger than in CMIP3 SST case. In the simulations with MIROC SST (Fig. 7g–i), precipitation increases over almost all the region except for Korea and the East China Sea. Simulations with MRI SST (Fig. 7j–l) show increase of precipitation around 30°N and decrease of precipitation to the south of 25°N. Changes over Japan are not statistically significant.

Figure 8 compares the precipitation change between the 20-km model and the 60-km model simulations for July. Area and amount of precipitation increase in MIROC SST simulations (Fig. 8e) to the south of 25°N is much larger than other simulations with different SSTs (Fig. 8c, d, f). This is partly due to the larger warming of SST projected by MIROC AOGCM (Fig. 2c), which leads to the larger holding capacity of water vapor in the atmosphere. Comparing the 20-km model result (Fig. 8a) and the average of all the 60-km model ensemble simulations (Fig. 8b), precipitation increases over the East China Sea, the Japan Sea and ocean to the south of Japan in both simulations. Also, precipitation increases over the Yangtze river valley in both simulations, but the region of statistically significant increase is smaller in the 20-km model.

Figure 9 shows the precipitation averaged over Japan region for July. All the simulations by the 20-km model and the 60-km model are plotted. In the present-day climate, simulated precipitations by the 60-km model are within the range of observations. Simulated precipitation by the 20-km model is overestimated. In the future climate, precipitation projected by the 20-km model increases relative to the present-day climate simulation by the 20-km model. Similar precipitation increases are found in the 60-km simulations. Two individual simulations by the 60-km model with MIROC SST (X mark) show larger

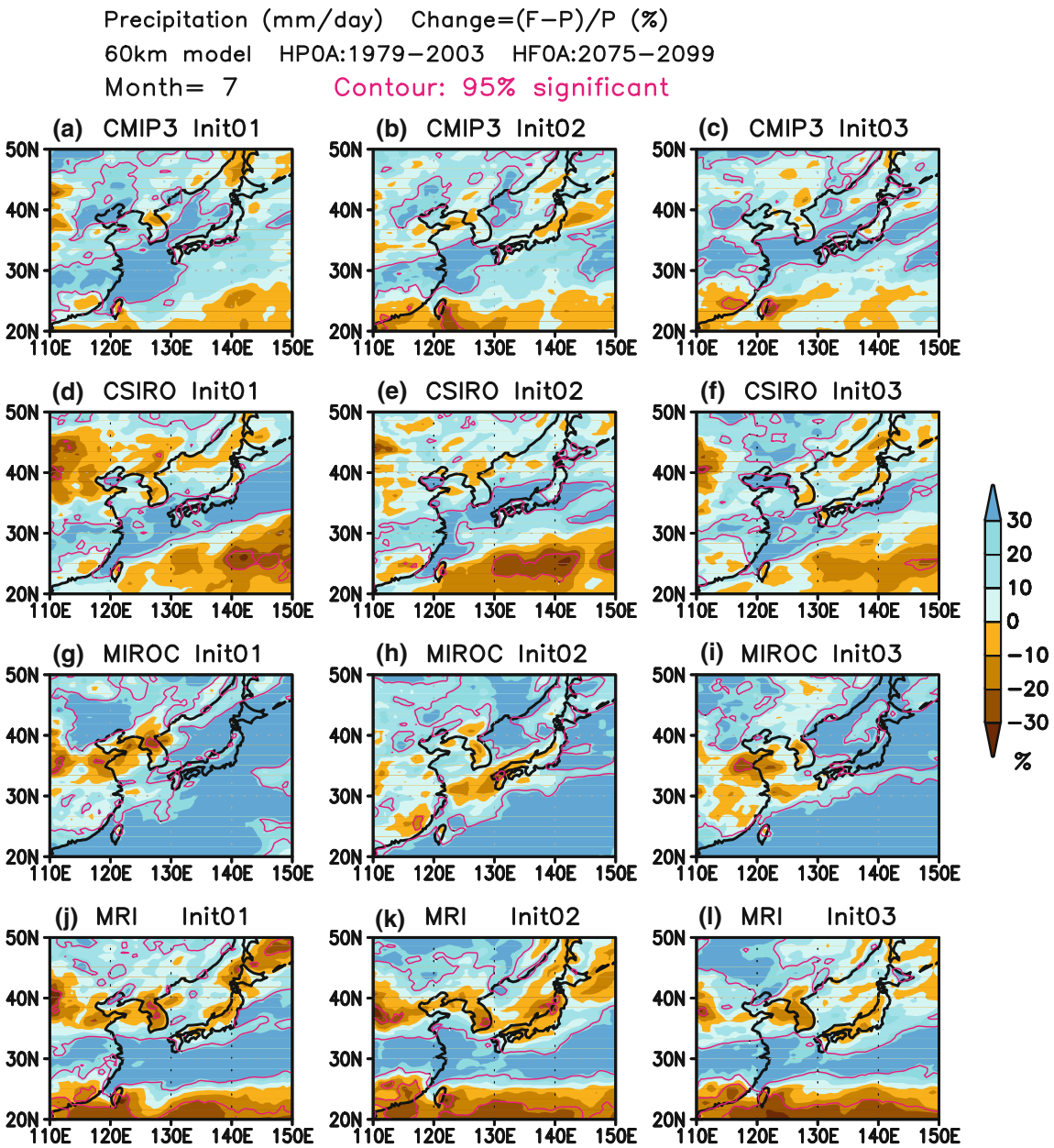

Fig. 7 Dependence of future changes in precipitation on SSTs (*rows*) and atmospheric initial conditions (*columns*) projected the 60-km model ensemble simulations for July. Unit is %. *Red contours* show the 95% confidence level. **a–c** (HF − HP)/HP. **d–f** (HF_CSIRO − HP)/HP. **g–i** (HF_MIROC − HP)/HP. **j–l** (HF_MRI − HP)/HP. The present-day climatology (HP) is the ensemble average of three simulations with three atmospheric initial conditions

precipitation than precipitation by any other simulations. These simulations correspond to precipitation change displayed by Fig. 7g and 7i. Again, this originates in the larger warming of SST projected by MIROC AOGCM (Fig. 2c).

Seasonal march of precipitation averaged over Japan is depicted in Fig. 10a. The future climate simulation by the 20-km model (SF) shows larger precipitation than the present-day climate simulation (SP) especially in July. Similar tendency is also found in the ensemble simulations by the 60-km models. Statistical significance of future change is shown by filled marks in Fig. 10b. Most of the precipitation change projected by the 20-km model are not statistically significant. In case of the 60-km model, increase of precipitation in July and August is much more evident than the 20-km. Simulations with MIROC SST show largest increase of precipitation in July and August with statistically significance. Increase of precipitation

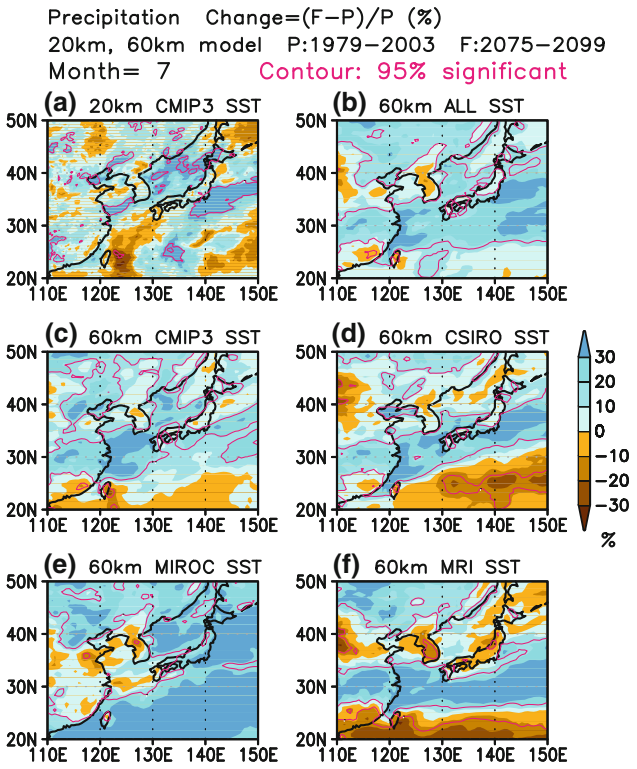

Fig. 8 Comparison of changes in precipitation between the 20-km model and the 60-km model ensemble simulations for July. Unit is %. **a** the 20-km model. Same as Fig. 5c. **b** The average of all ensemble simulations by the 60-km model (Fig. 7a–l). **c** The average of three ensemble simulations HF (Fig. 7a–c). **d** The average of three ensemble simulations HF_CSIRO (Fig. 7d–f). **e** The average of three ensemble simulations HF_MIROC (Fig. 7g–i). **f** The average of three ensemble simulations HF_MRI (Fig. 7j–l). Red contours show the 95% confidence level. In the calculation of *t*-value statistics for the-60 km model, the standard deviation (SD) for the present-day climate (HP) was estimated as the average of SDs of three individual simulations with different atmospheric initial conditions. SD for the future climate was also estimated as the average of SDs of consisting simulations. Sample size was set to 75 = 25 (years) × 3 (initial conditions) for the present-day climate simulations (HP), 300 = 25 (years) × 4 (SSTs) × 3 (initial conditions) for the all future climate simulations (**b**), and 75 = 25 (years) × 3 (initial conditions) for the future climate simulations (**c**–**f**)

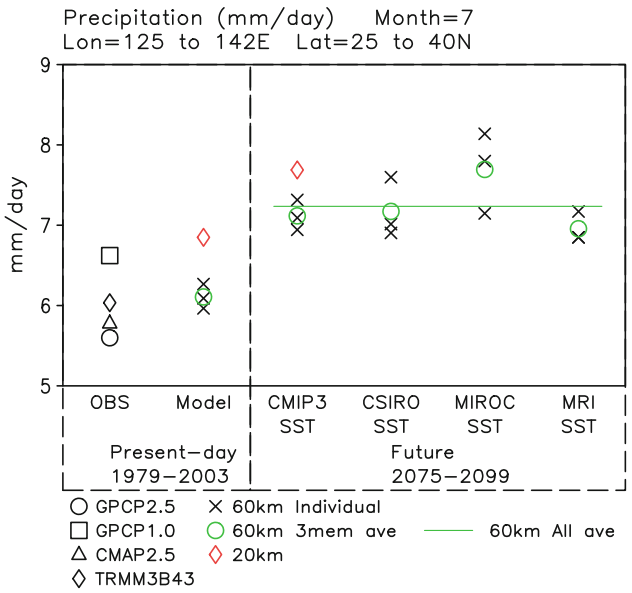

Fig. 9 Japan region (125–142°E, 25–40°N; The *box* in Fig. 3a) average precipitation for July. Unit is mm day^{-1}. *Left part* shows present-day climate. *Right part* shows future climate. Observational data are GPCP (2.5°, 1979–2003, 25 years), GPCP 1DD (1.0°, 1997–2008, 12 years), CMAP (2.5°, 1979–2003, 25 years) and TRMM 3B43 (0.25°, 1998–2008, 11 years). *Red diamonds* show the 20-km model simulations. *Black crosses* show the 60-km model simulations. *Green circles* show the ensemble average of three 60-km model simulations with different initial condition. *Green bar* shows the average of all ensemble simulations by the 60-km model

projected by the 20-km model and 60-km model in July is consistent with results shown by Figs. 7, 8 and 9. Tendency of precipitation increase in August suggests the delay in the termination of the Baiu season. This tendency of delay is consistent with the results of previous studies by CMIP3 AOGCMs (Kitoh and Uchiyama 2006) and by the 20-km model (Kusunoki et al. 2006; Kusunoki and Mizuta 2008).

8 Discussion

In order to interpret the changes in precipitation projected by models, horizontal transport of moisture is analyzed including Indian subcontinent. As one important part of Asia monsoon system, Indian monsoon exerts significant influences on the East Asian summer monsoon rainfall band. Figure 11 shows the changes in the vertically integrated water vapor flux and its convergence for July. In case of the 20-km model (Fig. 11a), the intensification of clockwise moisture transport over the western Pacific subtropical high is evident. The increases of north-eastward water vapor transport are found over China and the East China Sea. The geographical distribution of moisture convergence associated with the change in horizontal transport of moisture is almost similar to that of precipitation change over the Ease Asian region in Fig. 8a (110–150°E, 20–50°N). Precipitation change can be interpreted as the moisture convergence resulting from change in the horizontal transport of water vapor. Increase of clockwise moisture transport over the western Pacific subtropical high originates from the strengthening of the western Pacific subtropical high (figure not shown). This intensification of subtropical high is consistent with the results of previous studies using the 20-km model (Kusunoki et al. 2006; Kusunoki and Mizuta 2009) and studies with CMIP3 AOGCMs (Kitoh et al. 2009; Kimoto 2005). The increase of east-ward water vapor transport are

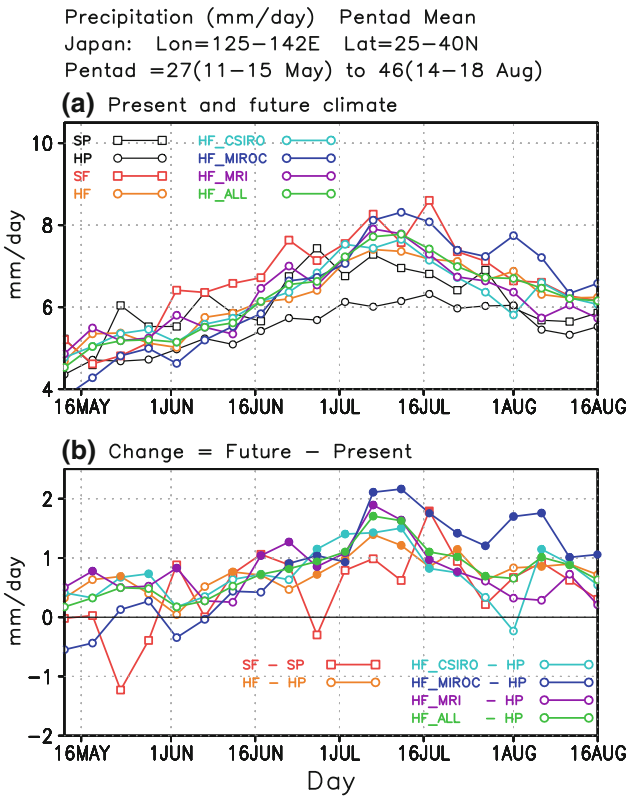

Fig. 10 Pentad mean time series of the precipitation averaged for Japan region (125–142°E, 25–40°N). The target region is indicated in Fig. 3a. The period is from pentad 27 (11–15 May) to 46 (14–18 August). Unit is mm day^{-1}. **a** The present-day and the future climate simulations. The ensemble averages of 60-km model simulations with three different initial condiitions are used. HF_ALL shows the average of all ensemble simulations by the 60-km model. **b** Changes in the future climate simulations. Filled mark means that changes are significant at the 95% level

found over India, Bay of Bengal and Indochina Peninsula, suggesting some influence of Indian summer monsoon upon the East Asian summer monsoon.

In case of the 60-km model (Fig. 11b), change in the convergence of moisture associated with change in horizontal water vapor transport show qualitatively similar distribution as the 20-km model (Fig. 11a). Change projected by the 60-km model with MIROC SST (Fig. 11e) is much different from other simulations (Fig. 11c, d, f) in that increase of moisture transport from the South China Sea, Indochina Peninsula and India is larger than the increase of clock wise moisture transport over the western Pacific subtropical high. Large moisture convergence associated with increase of moisture transport from the South China Sea and the increase of clock wise moisture transport over the western Pacific subtropical high results in the increase of precipitation over most part of the East Asia region. This is mainly due to the large increase of moisture contained in the atmosphere which is brought by the large warming of SST by MIROC AOGCM (Fig. 2c). In case of simulation with MRI SST (Fig. 11f), change in water vapor transport over India, India, Bay of Bengal and Indochina Peninsula is small and random, suggesting weak linkage between Indian summer monsoon and the East Asian summer monsoon.

9 Conclusion

A Global warming projection experiments were conducted using a 20-km mesh global atmospheric model, focusing on the change in the rain band of the East Asian summer monsoon. To assess the uncertainty of climate change projections, we performed ensemble simulations with the 60-km resolution model combining four different SSTs and three atmospheric initial conditions.

The results are summarized below:

1. In the present-day climate simulations, the 20-km model reproduces the rain band of the East Asian summer monsoon better than lower resolution models in terms of geographical distribution and seasonal march.
2. In the future climate simulation by the 20-km model, precipitation increases over the Yangtze River valley in May through July, Korean peninsula in May, and Japan in July. The termination of rainy season over Japan tends to be delayed until August.
3. Ensemble simulations by the 60-km model show that precipitation in the future climate for July increases over the Yangtze River valley, the East China Sea and Japan. These changes in precipitation are partly consistent with those projected by the 20-km model.
4. Simulations by the 20-km and 60-km models consistently show that in the future climate the termination of rainy season over Japan tends to be delayed until August.
5. The changes in the vertically integrated water vapor flux show the intensification of clockwise moisture transport over the western Pacific subtropical high. Most precipitation changes over the East Asia can be interpreted as the moisture convergence resulting from change in the horizontal transport of water vapor. Change in Indian summer monsoon partly contributes to the change in the East Asian summer monsoon.

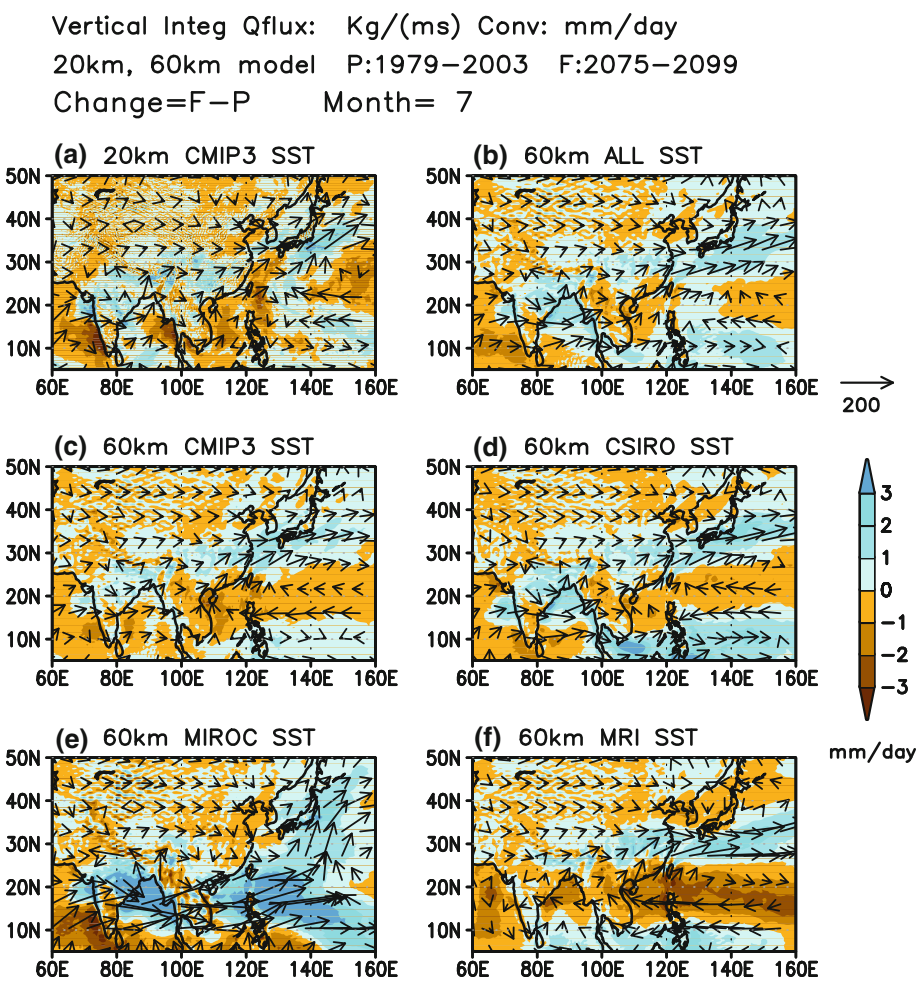

Fig. 11 Changes in vertically integrated water vapor flux (*arrow*, Kg m^{-1} s^{-1}) and its convergence (*color*, mm day^{-1}) for July. The unit of convergence is converted to mm day^{-1} assuming the density of liquid water as 1 g cm^{-3}. **a** the 20-km model. **b** The average of all ensemble simulations by the 60-km model. **c** The average of three ensemble simulations HF. **d** The average of three ensemble simulations HF_CSIRO. **e** The average of three ensemble simulations HF_MIROC. **f** The average of three ensemble simulations HF_MRI

Acknowledgments This work was conducted under the framework of the "Projection of the change in future weather extremes using super-high-resolution atmospheric models" supported by the KAKUSHIN Program of the Ministry of Education, Culture, Sports, Science, and Technology (MEXT). The calculations were performed on the Earth Simulator. We thank the anonymous reviewers whose valuable comments and suggestions greatly improved the manuscript.

References

Adler RF, Huffman GJ, Chang A, Ferrano R, Xie P-P, Janowiak J, Rudolf B, Schneider U, Curtis S, Bolvin D, Gruber A, Susskind J, Arkin P, Nelkin E (2003) The Version-2 Global Precipitation Climatology Preject (GPCP) monthly precipitation analysis (1979–Present). J Hydrometeor 4:1147–1167

Bengtsson L, Botzet M, Esch M (1996) Will greenhouse gas-induced warming over the next 50 years lead to higher frequency and greater intensity of hurricanes? Tellus 48A:57–73. doi: 10.1034/j.1600-0870.1996.00004.x

Habata S, Umezawa K, Yokokawa M, Kitawaki S (2004) Hardware system of the Earth Simulator. Parallel Comput 30:1287–1313. doi:10.1016/j.parco.2004.09.004

Huffman GJ, Adler RF, Morrissey MM, Curtis S, Joyce R, McGavock B, Susskind J (2001) Global precipitation at one-degree daily resolution from multi-satellite observations. J Hydrometeor 2:36–50

Huffman GJ, Adler RF, Bolvin DT, Gu G, Nelkin EJ, Bowman KP, Hong Y, Stocker EF, Wolff DB (2007) The TRMM Multisatellite Precipitation Analysis (TMPA): Quasi-global, multiyear, combined-sensor precipitation estimates at fine scales. J Hydrometeor 8:38–55

IPCC (Intergovernmental Panel on Climate Change) (2000) Special report on emissions scenarios. A special report of working group III of the intergovernmental panel on climate change. In: Nakićenović N, Alcamo J, Davis G, de Vries B, Fenhann J, Gaffin S, Gregory K, Grübler A, Yong Jung T, Kram T, La Rovere EL, Michaelis L, Mori S, Morita T, Pepper W, Pitcher H, Price L, Riahi K, Roehrl A, Rogner H-H, Sankovski A, Schlesinger M, Shukla P, Smith S, Swart R, van Rooijen S, Victor N, Dadi Z (eds). Cambridge University Press, Cambridge, UK, p 595

IPCC (2007) Climate change 2007: the physical science basis. Contribution of Working Group I to the fourth assessment report of the intergovernmental panel on climate change. In: Solomon S, Qin D, Manning M, Chen Z, Marquis M, Averyt KB, Tignor M, Miller HL (eds). Cambridge University Press, Cambridge, p 996

Kimoto M (2005) Simulated change of the East Asian circulation under global warming scenario. Geophys Res Lett 32:L16701. doi:10.1029/2005GL023383

Kitoh A, Uchiyama T (2006) Changes in onset and withdrawal of the East Asian summer rainy season by multi-model global warming experiments. J Meteor Soc Japan 84:247–258. doi:10.2151/jmsj.84.247

Kitoh A, Ose T, Kurihara K, Kusunoki S, Sugi M, KAKUSHIN Team-3 Modeling Group (2009) Projection of changes in future weather extremes using super-high-resolution global and regional atmospheric models in the KAKUSHIN Program: results of preliminary experiments. Hydrol Res Lett 3:49–53. doi:10.3178/HRL.3.49

Kusunoki S, Mizuta R (2008) Future changes in the Baiu rain rand projected by a 20-km mesh global atmospheric model: sea surface temperature dependence. SOLA 4:85–88. doi:10.2151/sola2008-022

Kusunoki S, Yoshimura Y, Yoshimura H, Noda A, Oouchi K, Mizuta R (2006) Change of Baiu rain band in global warming projection by an atmospheric general circulation model with a 20-km grid size. J Meteor Soc Japan 84:581–611. doi:10.2151/jmsj.84.581

Mizuta R, Oouchi K, Yoshimura H, Noda A, Katayama K, Yukimoto S, Hosaka M, Kusunoki S, Kawai H, Nakagawa M (2006) 20 km-mesh global climate simulations using JMA-GSM model. J Meteor Soc Japan 84:165–185. doi:10.2151/jmsj.84.165

Mizuta R, Adachi Y, Yukimoto S, Kusunoki S (2008) Estimation of the future distribution of sea surface temperature and sea ice using the CMIP3 multi-model ensemble mean. Tech Rep Meteorol Res Inst 56:28pp. http://www.mri-jma.go.jp/Publish/Technical/DATA/VOL_56/tec_rep_mri_56.pdf#page=5. Accessed 11 Nov 2010

Ninomiya K, Akiyama T (1992) Multi-scale features of Baiu, the summer monsoon over Japan and the East Asia. J Meteor Soc Japan 70:467–495

Rayner NA, Parker DE, Horton EB, Folland CK, Alexander LV, Rowell DP, Kent EC, Kaplan A (2003) Global analyses of sea surface temperature, sea ice, and night marine air temperature since the late nineteenth century. J Geophys Res 108(D14):4407. doi:10.1029/2002JD002670

Wang B, Ho L (2002) Rainy season of the Asian-Pacific summer monsoon. J Clim 15:386–398

Xie P, Arkin P (1997) Global precipitation: A 17 year monthly analysis based on gauge observations, satellite estimates and numerical model outputs. Bull Am Meteor Soc 78:2539–2558

Yamaguchi K, Noda A (2006) Global warming patterns over the North Pacific: ENSO versus AO. J Meteor Soc Japan 84:221–241. doi:10.2151/jmsj.84.221

Yatagai A, Arakawa O, Kamiguchi K, Kawamoto H, Nodzu MI, Hamada A (2009) A 44-year daily gridded precipitation dataset for Asia based on a dense network of rain gauges. SOLA 5:137–140. doi:10.2151/sola.2009-035

Yoshimura H, Matsumura T (2005) A two-time-level vertically-conservative semi-Lagrangian semiimplicit double Fourier series AGCM. CAS/JSC WGNE Res Activities Atmospheric Ocean Modeling 35:3.27–3.28